Magnetic tight binding and the iron-chromium enthalpy anomaly

Anthony T. Paxton
Atomistic Simulation Centre, School of Mathematics and Physics, Queen's University Belfast, Belfast BT7 1NN, United Kingdom

Michael W. Finnis
Department of Materials and Department of Physics, Imperial College London, Exhibition Road, London SW7 2AZ, United Kingdom
(Received 2 November 2007; published 30 January 2008)

We describe a self-consistent magnetic tight-binding theory based in an expansion of the Hohenberg-Kohn density functional to *second order*, about a non-spin-polarized reference density. We show how a *first order* expansion about a density having a trial input magnetic moment leads to a fixed moment model. We employ a simple set of tight-binding parameters that accurately describes electronic structure and energetics, and show these to be transferable between first row transition metals and their alloys. We make a number of calculations of the electronic structure of dilute Cr impurities in Fe, which we compare with results using the local spin density approximation. The fixed moment model provides a powerful means for interpreting complex magnetic configurations in alloys; using this approach, we are able to advance a simple and readily understood explanation for the observed anomaly in the enthalpy of mixing.

DOI: 10.1103/PhysRevB.77.024428 PACS number(s): 71.20.−b, 75.50.Bb

I. INTRODUCTION

There is much subtlety connected with itinerant magnetism in transition metals that one would, nevertheless, wish to capture in a simple model. Recently, an interatomic potential including magnetism has been proposed[1] which will prove very useful for molecular dynamics, but will not be able to describe electronic structure effects such as the competition between ferro- and antiferromagnetism, or the sudden collapse of the moment in hcp-Fe under pressure.[2–4] There are much greater difficulties attendant on interatomic potentials employing a term in the energy which is linear in the magnetic moment.[5,6] Almost certainly, a minimum requirement of a simple model is that it describes the electron kinetic energy. This is because intersite magnetic interactions are carried by the hopping matrix elements of the one-electron part of the Hamiltonian, not by intersite two-electron Coulomb integrals, and so Heisenberg and Ising models are not appropriate to discuss itinerant magnetism.[7,8] The tight-binding approximation, on the other hand, provides just such a description;[9–11] in its most economical form, it becomes a *bond order potential* recently described for transition metals by Drautz and Pettifor.[4] Whether a *magnetic* bond order potential will appear remains to be seen; as we will find below and as pointed out in Ref. 4, an accurate prediction of some magnetic effects requires quite detailed structure in the density of states near the Fermi level. Magnetic tight binding has been proposed many times using two slightly different self-consistent schemes. The first[2,12,13] is based on a rigid band approximation first used by Andersen *et al.*[2,14,15] in the context of the local spin density approximation (LSDA).[16] The non-spin-polarized density of states is allowed to split rigidly as a result of on-site exchange and correlation interactions, and an energy functional [Eq. (7) below] is minimized. This procedure may also be used in atomistic simulation if applied to the *local* density of states site by site, and provides a simple way to include effects such as magnetic pressure at crystal defects and site dependent magnetic moments.[17] A second more general approach is a self-consistent scheme in which the rigid band approximation is lifted and both the density of states and the exchange splitting are determined self-consistently.[3] We are motivated to recast this procedure into our recently proposed self-consistent polarizable ion tight-binding model,[11,18,19] based on an expansion of the Hohenberg-Kohn functional[20] to second order in a reference electron density. We will employ a non-spin-polarized input density, which may seem surprising but is consistent with the Stoner form of the LSDA, which expands the exchange correlation potential to linear order in the magnetic moment.[14–16]

We construct very simple tight-binding models for Cr, Fe, and Co, which we expect to be transferable to other transition metals and their alloys. Finally, we address an outstanding question in the thermodynamics of Fe-Cr alloys, namely, the anomalous negative enthalpy of mixing at the Fe-rich end of the phase diagram.[21] It is now well known that whereas over most of the concentration range Fe and Cr are immiscible,[22] at low concentrations Cr is soluble in Fe, with a negative enthalpy of mixing. An explanation based on a phenomenological Ising model has been proposed,[23] and a classical potential has been fitted to reproduce the phase diagram.[24] Recent LSDA calculations[25] revealed that Cr atoms favor clustering, except at low concentrations when there is a repulsive interaction between Cr impurities. Klaver *et al.*[25] pointed to this repulsive interaction in order to explain the negative to positive upturn in the enthalpy of mixing at concentrations in the range of 8–12 at. % Cr. Band structure arguments have been put forward based on densities of states within the coherent potential approximation,[26] but these were rather far removed from the actual densities, somewhat invalidating the conclusions. We are able to advance explanations for these phenomena using tight-binding calculations, which are remarkably close to our LSDA results and which give rise to a ready explanation easily understood within a fixed moment picture of itinerant magnetism.

The structure of the paper is as follows. In Sec. II, we describe how to include spin polarization into the self-consistent polarizable ion tight-binding model, and we de-

 ©2008 The American Physical Society

scribe how a fixed moment picture may be recovered from the same framework in Sec. III. In Sec. IV, we deduce parameters for a simple, transferable, nonorthogonal tight-binding model for transition metals. We apply this model to pure Fe and Cr in Sec. V, and to Co in Sec. VI. In Sec. VII, we apply the model to structural energetics of pure Fe. In Sec. VIII, we address the electronic structure of Fe-Cr alloys, and in Sec. IX, describe the use of a fixed moment model to predict the magnetic structure and energy. We propose an explanation of the enthalpy anomaly in Sec. X, and conclude in Sec. XI. In Appendix A, we show how an equivalent form of the electron-electron interaction energy to that derived in Sec. II may be obtained from a multiband Hubbard model as used in local density approximation (LDA)+U theory, which exposes the neglect of self-interaction correction in LSDA and our magnetic tight binding while indicating how this could be put back into a tight-binding scheme. In Appendix B, we describe nonorthogonal self-consistent tight binding; in particular, we show that, in this case, self-consistency leads to adjustment of the *hopping integrals* in addition to the on-site increments, and we illustrate the origin of additional contributions to the interatomic force arising from bond charges.

II. SELF-CONSISTENT TIGHT BINDING INCLUDING MAGNETISM

In our self-consistent polarizable ion tight-binding model, we express the electron Hamiltonian as

$$H = H_0 + H'.$$

The first term is the usual non-self-consistent tight-binding Hamiltonian of noninteracting electrons.[9] H' describes electron-electron interactions and is constructed so as to represent second order terms in the expansion of the Hohenberg-Kohn density functional about a reference density ρ_{in}.[11] We take it that ρ_{in} is constructed by overlapping spherical, neutral, non-spin-polarized atomic charge densities. H_0 is then the Hamiltonian whose effective potential is generated by ρ_{in}.[11] We introduce a spin density $\rho=\Sigma_\sigma \text{Tr}\,\hat{\rho}^\sigma = \Sigma_\sigma \rho^\sigma = \rho^+ + \rho^-$, the electron spin taking the value $\sigma = \pm 1$ in units of $\frac{1}{2}\hbar$. Minimization of the Hohenberg-Kohn functional leads to two Kohn-Sham equations,[27] in atomic Rydberg units,

$$(-\nabla^2 + V_{\text{eff}}^\sigma)\psi^\sigma = \varepsilon\psi^\sigma$$

in an effective potential

$$V_{\text{eff}}^\sigma = V_{\text{xc}}^\sigma + V_H + V_{\text{ext}},$$

where V_H is the Hartree potential, V_{ext} the external potential due to the ions, and

$$V_{\text{xc}}^\sigma = \frac{\delta E_{\text{xc}}}{\delta \rho^\sigma} \tag{1}$$

is the exchange and correlation potential. In the absence of a magnetic field (which we could include as a Zeeman term in V_{ext}), this is the only term which is spin dependent. The corresponding Hohenberg-Kohn-Sham energy functional is (we may suppress the symbol $d\mathbf{r}$ under an integral sign)

$$E^{\text{HKS}} = \sum_{\substack{\sigma,n\mathbf{k} \\ \text{occ.}}} \langle \psi_{n\mathbf{k}}^\sigma | \hat{T} + V_{\text{eff}}^\sigma | \psi_{n\mathbf{k}}^\sigma \rangle - \sum_\sigma \int \rho^\sigma V_{\text{xc}}^\sigma - E_H + E_{\text{xc}}[\rho^+, \rho^-] + E_{ZZ},$$

in which $\hat{T}$ is the kinetic energy operator, E_H is the Hartree energy, and E_{ZZ} is the ion-ion interaction. This is expanded about the reference non-spin-polarized densities

$$\rho_{\text{in}}^+ = \rho_{\text{in}}^- = \frac{1}{2}\rho_{\text{in}},$$

and we define

$$\delta\rho^\sigma = \rho^\sigma - \rho_{\text{in}}^\sigma, \quad \delta\rho = \rho - \rho_{\text{in}} = \delta\rho^+ + \delta\rho^-.$$

The exchange and correlation energy is expanded to second order in $\delta\rho^\sigma$ to give

$$E_{\text{xc}}[\rho^+, \rho^-] = E_{\text{xc}}^{\text{in}} + \sum_\sigma \int V_{\text{xc}}^{\text{in}} \delta\rho^\sigma + \frac{1}{2}\sum_{\sigma\sigma'} \int\int \delta\rho^\sigma \frac{\delta^2 E_{\text{xc}}}{\delta\rho^\sigma \delta\rho^{\sigma'}} \delta\rho^{\sigma'} + \cdots.$$

The Hohenberg-Kohn total energy, exact apart from the neglect of terms higher than second order in E_{xc}, is[28]

$$E^{(2)} = \sum_{\substack{\sigma,n\mathbf{k} \\ \text{occ.}}} \langle \psi_{n\mathbf{k}}^\sigma | H_0 | \psi_{n\mathbf{k}}^\sigma \rangle - \int \rho_{\text{in}} V_{\text{xc}}^{\text{in}} - E_H^{\text{in}} + E_{\text{xc}}^{\text{in}} + E_{ZZ} + \frac{1}{2}\int d\mathbf{r} \int d\mathbf{r}' \left\{ e^2 \frac{\delta\rho(\mathbf{r})\,\delta\rho(\mathbf{r}')}{|\mathbf{r}-\mathbf{r}'|} + \sum_{\sigma\sigma'} \delta\rho^\sigma(\mathbf{r}) \frac{\delta^2 E_{\text{xc}}}{\delta\rho^\sigma(\mathbf{r})\,\delta\rho^{\sigma'}(\mathbf{r}')} \delta\rho^{\sigma'}(\mathbf{r}') \right\}. \tag{2}$$

The first two lines amount to the Harris-Foulkes functional.[11,29,30] The second line is represented by a pairwise repulsive energy, E_{pair}, in the usual tight-binding models. In our self-consistent polarizable ion tight-binding model, we approximate the third line as the electrostatic interaction energy between point multipole moments of the charge transfer. The fourth line is the extension of the on-site electron-electron interaction Hubbard term to the spin-polarized case, and we now examine this term in more detail using Eq. (1) by writing

$$E_2^U = \frac{1}{2}\sum_{\sigma\sigma'} \int\int \delta\rho^\sigma \frac{\delta V_{\text{xc}}^\sigma}{\delta\rho^{\sigma'}} \delta\rho^{\sigma'}.$$

Here, we have suppressed the $\mathbf{r}$ dependence, first, because all off-diagonal Coulomb terms are relegated to the Madelung energy [the third line in Eq. (2)] in our tight-binding model, recognizing that itinerant magnetism is a consequence of *on-site* exchange and correlation;[31] and second, because in our

tight-binding model, we will be using a local orbital basis to represent the spin density.

The quantity

$$\frac{\delta V_{\mathrm{xc}}^{+}}{\delta \rho^{-}} = \frac{\delta V_{\mathrm{xc}}^{-}}{\delta \rho^{+}} \equiv U \tag{3}$$

is the direct Coulomb, correlation only, interaction strength between unlike spins described by the Hubbard U parameter. On the other hand, the quantity

$$\frac{\delta V_{\mathrm{xc}}^{+}}{\delta \rho^{+}} = \frac{\delta V_{\mathrm{xc}}^{-}}{\delta \rho^{-}} \equiv U - I \tag{4}$$

reflects the lowering of the electron-electron interaction through exchange by an amount I, here called the Stoner parameter. Because of the Pauli principle, electrons with like spins are kept further apart and so their electrostatic Coulomb repulsion is, on average, weaker than for unlike spin electrons. This is the origin of Hund's rule as well as spin polarization of itinerant electrons. Using these definitions of U and I, we can write down E_2^U in terms of the total density and the magnetic moment [Eq. (5) below]. First, we note that the magnetic moment m is

$$m = \rho^{+} - \rho^{-} = \delta\rho^{+} - \delta\rho^{-} = \delta m$$

since the input density is non-spin-polarized. We then find, using Eqs. (1), (3), and (4),

$$\frac{\delta^2 E_{\mathrm{xc}}}{\delta \rho^2} = U - \frac{1}{2} I,$$

whereas[32,33]

$$I = -2\frac{\delta^2 E_{\mathrm{xc}}}{\delta m^2},$$

where the second derivatives are to be evaluated at the input density, i.e., $m=0$.

We also have

$$\delta\rho^{+} = \frac{1}{2}(\delta\rho + \delta m), \quad \delta\rho^{-} = \frac{1}{2}(\delta\rho - \delta m)$$

from which we readily obtain the central result of this section,

$$E_2^U = \frac{1}{2} U \delta\rho^2 - \frac{1}{4} I \delta\rho^2 - \frac{1}{4} I m^2. \tag{5}$$

Only the first two terms survive in the non-spin-polarized model described previously.[11,18,19] An associated expression may be obtained from the LDA+U formalism as demonstrated in Appendix A. Finally, we give the expression for the tight-binding total energy including the magnetic terms,

$$E_{\mathrm{tot}} = E_1 + E_2 \tag{6}$$

with

$$E_1 = \sum_{\sigma} \mathrm{Tr}[\hat{\rho}^{\sigma} H_0] + E_{\mathrm{pair}}$$

and

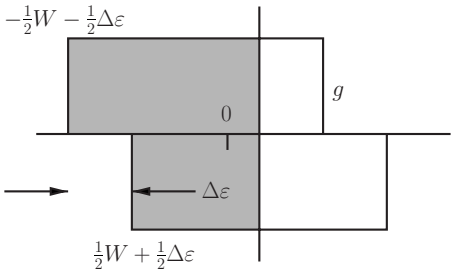

FIG. 1. To illustrate the simple rectangular density of states model of ferromagnetism. A density of states which is constant and equal to g between band edges $\pm\frac{1}{2}W$ is split by exchange into majority and minority spin densities by an amount proportional to the moment, m. (This can be achieved by flipping the spins of $\frac{1}{2}m$ electrons and realigning the Fermi levels to a common value.) By construction, we have $\Delta\varepsilon = m/g = Im$. (After Fig. 8.12c of Ref. 10.)

$$E_2 = \frac{1}{2}\sum_{\mathbf{R}} \left\{ \sum_{L} Q_{\mathbf{R}L} V_{\mathbf{R}L}^{M} + \left(U_{\mathbf{R}} - \frac{1}{2} I_{\mathbf{R}} \right) \delta q_{\mathbf{R}}^2 - \frac{1}{2} I_{\mathbf{R}} m_{\mathbf{R}}^2 \right\}$$

in which $\hat{\rho}^{\sigma}$ is the spin density matrix, $\mathbf{R}$ labels atomic sites, and $\delta q_{\mathbf{R}}$ and $V_{\mathbf{R}L}^{M}$ are as defined in Eqs. (B1) and (B2) in Appendix B. There are no additional contributions to the interatomic force due to spin polarization.[3]

III. RIGID BAND AND FIXED MOMENT MODELS

In the previous section, we expanded the Hohenberg-Kohn total energy to *second order* around a non-spin-polarized reference density. This is the self-consistent tight-binding model that is closest to the LSDA. Alternatively, one may expand about a spin-polarized density having a nonzero trial magnetic moment.[35] We now show that, in this case, an expansion to *first order* leads to a fixed moment model similar to the well known rigid band Stoner-Slater model[31,36–38] (usually referred to as just the "Stoner model"). We recall first that the Stoner model is most readily illustrated[10,39,40] using the rectangular density of states, representing the d band in a transition metal shown in Fig. 1. We imagine that majority spin electrons see an exchange and correlation potential lower than that seen by minority electrons by an amount proportional to the magnetic moment, m; the proportionality constant, I, being the "Stoner parameter." (Stoner uses the symbol α for this; I is Slater's usage.[31]) Then the rectangular bands are split by $\pm\frac{1}{2}\Delta\varepsilon = \pm\frac{1}{2} Im$ and the change in band (kinetic) energy due to magnetization is

$$\begin{aligned}\Delta E_{\mathrm{band}} &= \left(\int_{-(1/2)W-(1/2)\Delta\varepsilon}^{\varepsilon_F} g\varepsilon d\varepsilon + \int_{-(1/2)W+(1/2)\Delta\varepsilon}^{\varepsilon_F} g\varepsilon d\varepsilon \right. \\ &\quad \left. - 2\int_{-(1/2)W}^{\varepsilon_F} g\varepsilon d\varepsilon \right) \\ &= -\frac{1}{4} g I^2 m^2,\end{aligned}$$

using $\Delta\varepsilon = Im$. In this estimate of the magnetic energy, the electron-electron interaction energy, $-\frac{1}{4} Im^2$, has been double counted, so it is subtracted to give

$$\Delta E_{\mathrm{mag}} = \frac{1}{4} I m^2 (1 - Ig),$$

which is negative as long as $Ig > 1$, which is the simplest statement of the Stoner criterion.[36] This particular model is pathological because ΔE_{mag} has no minimum as a function of m. This is a symptom of using a constant density of states, so that the kinetic energy is quadratic in m; that is, the fourth order term which is responsible for stabilizing the ferromagnetic state is missing in the absence of structure in the density of states.

According to Slater,[31] ferromagnetism arises from a competition between kinetic energy and on-site Coulomb electron-electron interactions. For an arbitrarily shaped density of states, the kinetic energy increases compared to the spin-paired state when down-spin electrons are spin flipped, since they must then be promoted into unoccupied states above the Fermi level. To develop a magnetic moment, m, charge is transferred across the Fermi surface in small increments dm, each increment costing more energy than the last as the down-spin states are depleted below the Fermi level and need to be taken from lower energy states and placed as up-spin electrons in higher energy states as these become successively occupied above the Fermi level. Generally speaking, the larger the density of states near the Fermi level, the smaller is the energy penalty involved. To counter this increase in kinetic energy, there will be a decrease in energy due to a Hund's rule like exchange interaction, and Slater[31] argues that this takes the form $-\frac{1}{4} I m^2$. Hence, the total change in energy upon forming a magnetic moment m is[2,12,15,32,39]

$$\Delta E_{\mathrm{mag}}(m) = \frac{1}{2} \int_0^m \frac{m' dm'}{\bar{g}(m')} - \frac{1}{4} I m^2, \tag{7}$$

which is clearly stationary at a generalized Stoner condition, namely, $I\bar{g}(m) = 1$, where $\bar{g}(m)$ is the density of states averaged over the energy range spanned by flipping the $\frac{1}{2}m$ spins; see Fig. 30 in Ref. 14.

This is a rigid band model, requiring us to know only the nonmagnetic density of states. Now we generalize this to a "magnetic fixed moment model." We can obtain an analogous expression for ΔE_{mag} from a Harris-Foulkes functional, namely, the first two lines of Eq. (2). In contrast to the second order theory in which the input density is non-spin-polarized, let us consider a trial density which can be varied by changing its magnetic moment while not affecting the total charge density.[35] We now have $m_{\mathrm{in}} = \rho_{\mathrm{in}}^{+} - \rho_{\mathrm{in}}^{-}$ and the trial Hamiltonian is

$$H^{\sigma} = H_0 + V_{\mathrm{xc}}^{\sigma}[\rho_{\mathrm{in}}],$$

where

$$V_{\mathrm{xc}}^{\sigma}[\rho_{\mathrm{in}}] = -\frac{1}{2} \sigma I m_{\mathrm{in}}$$

so that $\sigma = +1$ are the majority spins (i.e., see a lower exchange and correlation potential). We now evaluate the first order total energy,

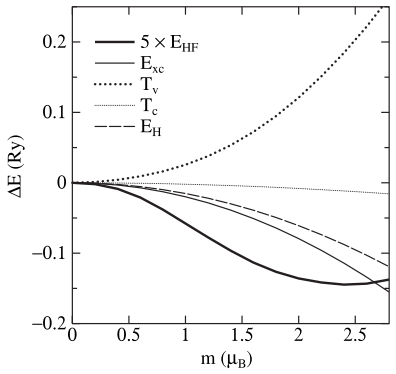

FIG. 2. Contributions to the total energy in a LMTO (Ref. 41) calculation for pure bcc-Fe relative to their values at $m=0$. This is the Harris-Foulkes energy E_{HF} (Refs. 29 and 30) as a function of the fixed magnetic moment of the input density ρ_{in}. T_c and T_v are core and valence kinetic energies, and E_H is the Hartree energy. We find that E_{xc} is almost exactly quadratic and, hence, its curvature is independent of m. Its curvature here is −0.04, giving $I=80$ mRy compared to the value 65 mRy (Refs. 14, 44, and 45) using both Janak's method (Ref. 34) and that of Poulsen *et al.* (Ref. 44), and 68 mRy as calculated by Gunnarsson (Ref. 16). The fourth order term in E_{HF} which leads to a minimum at the observed moment comes from the kinetic energy.

$$E^{(1)}(m_{\mathrm{in}}) = \sum_{\substack{\sigma,n\mathbf{k} \\ \mathrm{occ.}}} \langle \psi_{n\mathbf{k}}^{\sigma} | H^{\sigma} | \psi_{n\mathbf{k}}^{\sigma} \rangle - \sum_{\sigma} \int \rho_{\mathrm{in}}^{\sigma} V_{\mathrm{xc}}^{\sigma}[\rho_{\mathrm{in}}] - E_{\mathrm{H}}^{\mathrm{in}} + E_{\mathrm{xc}}^{\mathrm{in}} + E_{ZZ}.$$

When we compare this to its value when $m_{\mathrm{in}}=0$, we obtain

$$\Delta E_{\mathrm{mag}}(m_{\mathrm{in}}) = \Delta E_{\mathrm{band}}(m_{\mathrm{in}}) + \frac{1}{4} I m_{\mathrm{in}}^2 \tag{8}$$

after evaluating the double counting in view of the fact that only the moment and not the density differ in the two cases, and using $\Delta E_{\mathrm{xc}}^{\mathrm{in}} = -\frac{1}{4} I m_{\mathrm{in}}^2$.

As an illustration, we show in Fig. 2 how a Harris-Foulkes energy varies with moment in pure bcc-Fe. Here, we have constructed an input density by superimposing free atoms[46,47] having a given magnetic moment so that the moment of the input density is a trial m_{in}. We then evaluate the Harris-Foulkes total energy functional and plot it against m_{in}. This is not a rigid band, but a fixed moment calculation; it serves to illustrate how the individual contributions to the energy vary with m_{in}. In particular, note that the kinetic energy increases, having both second and fourth order terms in m_{in}, while the exchange and correlation energy is found to be strictly quadratic. This is consistent with the Stoner picture and serves to show that the Stoner parameter I is independent of the moment and so may be taken as the same quantity in both Eqs. (6) and (8). Our estimate of I is, of course, not as good as a fully self-consistent calculation as we indicate in the caption of Fig. 2.

We will use Eq. (6) to calculate density of states and total energy in Secs. V–VIII. The fixed moment picture is particularly useful in interpreting complex magnetic structures and

TABLE I. Parameters of our tight-binding model. Atomic Rydberg units are used throughout.

	$ss\sigma$		$sp\sigma$		$pp\sigma$		$sd\sigma$		$pd\sigma$		$dd\sigma$			
	f_0	s_0	f_0	s_0	f_0	s_0	f_0	s_0	f_0	s_0	f_0	s_0	B	I
Cr	−0.75	0.5	0.5	−1.0	1.0	−0.1	−0.12	0.8	−0.5	0	0.18	0		0.050
Fe	−0.75	0.5	0.5	−1.0	1.0	−0.1	−0.12	0.8	−0.5	0	0.12	0	340	0.055
Co	−0.75	0.5	0.5	−1.0	1.0	−0.1	−0.12	0.8	−0.5	0	0.10	0	250	0.080

arriving at an explanation of the enthalpy anomaly. Therefore, in Secs. IX and X, we employ Eq. (8) to find the total energy.

IV. TIGHT-BINDING MODEL

Our tight-binding model is specified by distance dependent matrix elements of the Hamiltonian and overlap, by Hubbard U and Stoner I parameters, and by a repulsive pair potential. We are motivated to employ the simplest possible scheme so as to maximize its predictive power relative to its complexity.[11] Our starting point is the tight-binding theory of transition metals of Spanjaard and Desjonquères,[48] who proposed a universal, orthogonal scheme in which Hamiltonian matrix elements have the form $f_0 e^{-qd}$ and the pair potential takes the form Be^{-pd}, where d is the bond length. These are intended to extend to nearest neighbors only in fcc and hcp metals, and to second neighbors in the bcc structure. Spanjaard and Desjonquères found a universal ratio $p/q=2.95$ that fits well to the binding energy curve of Rose *et al.*[49] We have found this to be an excellent model for transition metals using an orthogonal basis of d electrons[50] and adopting the canonical ratio for the three quantities f_0, namely,

$$dd\sigma:dd\pi:dd\delta = -6f_0:5f_0:-2.2f_0,$$

Spanjaard and Desjonquères provided values of the product qd_0, where d_0 is the equilibrium bond length, for most transition metals. Therefore, the only adjustable parameters are f_0, which we adjust to the bandwidth calculated in the LDA, and the parameter B, which we adjust to obtain the correct atomic volume (or lattice constant). This simple model having two adjustable parameters then gives a good account of structural stability and elastic constants.[50]

For a number of reasons, we wish to go beyond this very simple scheme in three respects. (i) We will extend the range of the exponentially decaying interactions; specifically, we encompass 58 neighbors in the bcc lattice. This has the attraction of employing an energy surface without discontinuities in a molecular dynamics simulation. Furthermore, we have found this necessary to obtain a faithful reproduction of the LDA density of states. (ii) For this latter reason, we also prefer to include s and p electrons in the basis, and (iii) to adopt a nonorthogonal basis. We see a number of attractions from the inclusion of overlap which we discuss in Appendix B (see also the caption to Fig. 4). It is, furthermore, known that the neglect of sd hybridization leads to an overestimation of the magnetic moment of Fe.[17,44,51] Our procedure for obtaining the additional parameters is again motivated by simplicity, and we adjusted the additional matrix elements to obtain a close comparison between the LDA and tight-binding density of states in bcc Fe. Thereafter, we merely adjusted f_0 to allow for the differences in d-band width across the transition series. We use the same exponent in the overlap matrix elements as in the Hamiltonian, but with a different prefactor, they thereby take the form $s_0 e^{-qd}$. We use $qd_0^{bcc}=3$ for all dd interactions, otherwise we set $q=0.5$ bohr^{-1}. We deviated from the canonical ratios in the nonorthogonal case:

$$dd\sigma:dd\pi:dd\delta = -6f_0:5f_0:-2.2f_0,$$

and, furthermore, used the ratio

$$pp\sigma:pp\pi = 2:-1.$$

We fix the on-site energy levels of the s and p atomic levels at 0.2 and 0.45 Ry, respectively, relative to the d level. The remaining parameters are shown in Table I.

Our values of the Stoner I are essentially those calculated by Gunnarsson and others.[14,16,34,44,45,52] However, we adjust these to obtain magnetic moments in agreement with the LSDA.

Figure 3 illustrates the match between LDA and tight-binding densities of states in the nonorthogonal and orthogonal d-only tight-binding models. Note that the canonical model is quite adequate in describing the essential features, namely, the t_{2g} (xy,yz,zx) bonding and e_g (x^2-y^2,z^2-r^2) antibonding manifolds which stabilize the bcc structure at half band filling and the large density of states at the Fermi level, $g(\varepsilon_F)$, which is responsible for the ferromagnetic instability. To place the Fermi level exactly at the peak, it is necessary to choose the number of d electrons, N_d, as an additional parameter in the d-only tight-binding model; we set $N_d=6$. However, the three peak structure typical of bcc transition metals and the smooth "U-shaped" pseudogap are less faithfully reproduced in the canonical model.

V. FERRO- AND ANTIFERROMAGNETISM IN PURE IRON AND CHROMIUM

It is quite clear that both canonical and spd tight-binding models predict ferromagnetism in Fe based on the Stoner criterion, $Ig(\varepsilon_F)>1$, which in the simplest rectangular band models of Friedel[39] and Pettifor[40] is $I/W>1/5$, where W is the width of the d band.[10] In Fig. 4, we show the self-consistent tight-binding density of states compared to the LSDA. We find a self-consistent magnetic moment of $2.18\mu_B$. The density of states of Cr is, of course, of practi-

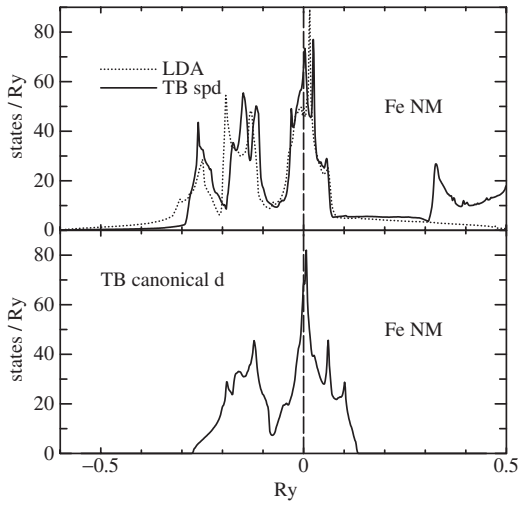

FIG. 3. Density of states of nonmagnetic Fe using two tight-binding models. The upper panel shows the nonorthogonal model having the parameters shown in Table I; the dotted line shows the LDA density of states. The lower panel shows the density of states in the canonical *d*-band tight-binding model.

cally the same shape as that of Fe, but the Fermi level falls inside the pseudogap. In Pettifor's *skewed* rectangular *d*-band theory,[10,40] antiferromagnetism is predicted if

$$\frac{I}{W} > \left[\frac{3}{10}N_d(10-N_d)\right]^{-1}.$$

In this theory, the analogy is made between an *AB* binary alloy and an antiferromagnetic crystal having two sublattices, as does the bcc structure. In the alloy, electrons will see a lower potential, say, at the *A* site, where the on-site energy level is lower than at the *B* site by an amount $\Delta\varepsilon$. In the common band model, this leads to a skewing of the simple rectangular density of states, so that lower energy eigenvalues are generally associated with the *A* site and vice versa. In this picture, electrons in the lower energy single particle states spend more time at the *A* site, while overall charge neutrality is maintained.[53] In the antiferromagnetic case (Fig. 5), one says that up-spin electrons see a lower exchange potential at one sublattice and the down spin at the other. Each of their on-site energies is lowered through the exchange interaction (Hund's rule) by an amount $\Delta\varepsilon = Im$, if I is sufficiently large, which favors aligned spins. Figure 6 shows that this effect is predicted in the self-consistent tight-binding model, and compares the resulting density of states with the LSDA. The local antiferromagnetic moment m in the tight-binding model is predicted to be $0.74\mu_B$, in close agreement with the $0.70\mu_B$ estimated from the LSDA spin density.

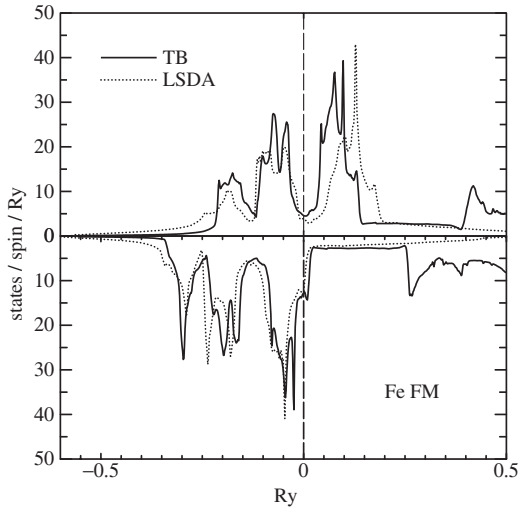

FIG. 4. Density of states in ferromagnetic Fe using the *spd* tight-binding model and compared with a LSDA calculation. The upper panel shows the minority and the lower panel the majority spins. Note that in an *orthogonal* tight-binding model, even using the fully self-consistent scheme of Sec. II, the two densities of states would be identical, only rigidly shifted. The inclusion of an overlap breaks this symmetry, and it is seen here that this additional freedom acts significantly to improve the comparison with the LSDA.

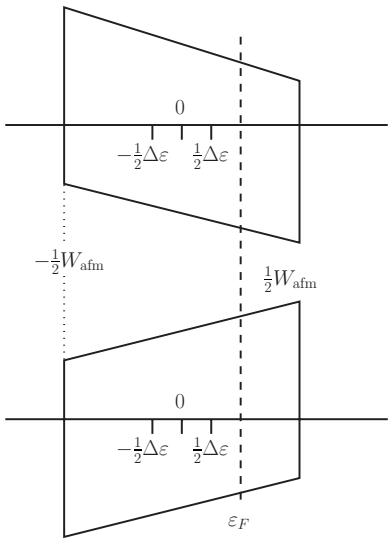

FIG. 5. Illustration of Pettifor's skewed rectangular band model of antiferromagnetism. The upper and lower figures show the densities of states on the two sublattices. A single one of these describes the situation in an *AB* alloy in which the electrons see a lower potential, say, at the *A* atom, whose density of states is accordingly skewed toward lower eigenvalues as in the upper density of states of the top diagram. In the antiferromagnetic analogy, on each sublattice the majority spin electrons see a lower potential due to exchange interactions, they spend more time at that site and the density of states is accordingly skewed. Spin up are the majority electrons at one sublattice, spin down at the other; hence the two diagrams, one for each sublattice. (After Fig. 8.12b of Ref. 10)

VI. TRANSFERABILITY TO COBALT

We begin the discussion of energetics with the application of the Spanjaard and Desjonquères model to Co. The approach we have taken is to adjust the parameter f_0 only to match the *d*-bandwidth of nonmagnetic bcc-Co calculated in

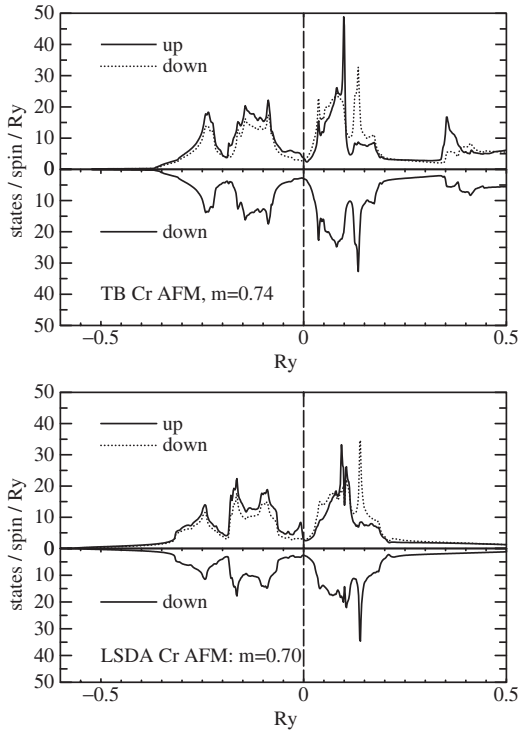

FIG. 6. Density of states in antiferromagnetic Cr showing both the *spd* tight-binding model and a LSDA calculation. In the upper panels are shown both the up spins and the down spins from the lower panel reflected in the *x* axis to reveal the lower density of states compared to the up spin. The reverse situation pertains on the other sublattice.

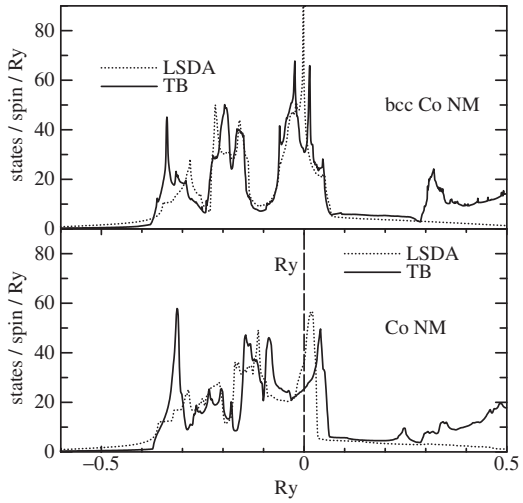

FIG. 7. Density of states in nonmagnetic Co: bcc (upper figure) and hcp (lower figure). Dotted lines show the LDA densities of states. Note that the parameters generated for the bcc structure transfer well to the observed hcp structure.

the LDA. The resulting density of states is shown in Fig. 7, which also shows the density of states in hcp-Co to demonstrate the transferability of the band parameters to the observed structure of Co.

The remaining parameter, B, that enters the pair potential was fitted to the calculated lattice constant of nonmagnetic bcc-Co. Table II shows the results of calculations of both bcc and hcp Co. The model is clearly remarkably predictive and argues strongly for the essential correctness of the Spanjaard and Desjonquères approach coupled to the second order Slater–Stoner theory. Particularly, note that the tight-binding correctly predicts the stability of the hcp over the bcc structure and also renders rather well the bulk moduli, both in magnetic and nonmagnetic forms. In connection with the Stoner I parameter, we note firstly that the value, 68 mRy, quoted for the LSDA is not, of course, an input into the calculation but this is the number calculated by other authors using the LSDA approach.[14] Second, we note that we tried two values in the tight-binding model: $I=80$ mRy gives a better value of the magnetic moment in bcc-Co, whereas this value gives a negative magnetic energy for hcp-Co, thus predicting this phase to be nonmagnetic. Increasing I to 85 mRy corrects this, but overstates the moment in bcc-Co.

VII. PHASE STABILITY IN IRON

We continue to look at the energetics by examining how the simple Spanjaard and Desjonquères model describes the stability of the close packed structures in Fe. This has been addressed in detail recently,[3] so for brevity we discuss only the bcc and hcp structures at two atomic volumes, $V/V_0=1$ and 0.88, where $V_0=11.82$ Å^3 is the experimental atomic volume of bcc-Fe and the transition to hcp-Fe is observed[54] to occur at about $V/V_0=0.88$. Table III shows that the predictions are less accurate than in the case of Co. We recall that very careful studies of the energetics in the LSDA have been made by Bagno *et al.*[55] and by Stixrude *et al.*[56] Their conclusions are that at $V/V_0=1$, the most stable phase is ferromagnetic bcc-Fe, but that the energy volume curve for antiferromagnetic hcp-Fe intersects that for bcc-Fe and has a minimum at a lower energy at $V/V_0\approx 0.88$. Hence, the global prediction of the LSDA is that hcp is the stable phase having a greater than ambient density. It is well known that this anomaly is removed by use of the so-called generalized gradient approximation (GGA), although Bagno *et al.* pointed out that this is probably merely a coincidence arising from the GGA favoring both larger atomic volumes and larger magnetic moments as a general rule. As can be seen in Fig. 8, our tight-binding model rather closely follows the LSDA, but fails to reproduce the stability of bcc-Fe even at the ambient atomic volume. Table III shows also the predicted magnetic moments and bulk modulus. Note that we have used the ideal axial c/a ratio for hcp at $V/V_0=1$, but its measured value at $V/V_0=0.88$.

Maybe it is not surprising that this very simple tight-binding model fails to describe the energetics of Fe. This is a very subtle problem even for the LSDA. The solution within tight binding is rather simple, however, as has been demonstrated recently, and requires the use of a more complicated pair potential.[3] This is consistent with the observations of Bagno *et al.*[55] concerning the role of the GGA, and need not concern us further here, since in what follows we will discuss electronic structure and leave aside the question of structural energetics.

TABLE II. Energetic data for Co, comparing tight-binding and LSDA calculations. Note that the only fitted values are the atomic volume of bcc-Co, although the Stoner I has also been adjusted to agree with the LSDA moments. V/V_0 is the atomic volume compared to experiment; $\Delta E_{h\text{-}b}$ is the energy of the hcp relative to the bcc phase; m is the magnetic moment; ΔE_{mag}, the "magnetic energy," is the calculated energy difference between magnetic and nonmagnetic phases; and K is the bulk modulus.

	I (mRy)	V/V_0	$\Delta E_{h\text{-}b}$ (mRy)		m (μ_B)		ΔE_{mag} (mRy)		K (Mbar)		
			TB	LSDA	TB	LSDA	TB	LSDA	TB	LSDA	Expt.
bcc	0	0.896				0 NM				2.94	
bcc	0	0.896			0 NM				3.04		
bcc	68	0.935				1.67 FM		18		2.52	
bcc	80	0.933			2.08 FM		18		2.81		
bcc	85	0.935			2.16 FM		22		2.82		
hcp	0	0.878		−18		0 NM			3.11		
hcp	0	0.875	−30		0 NM					3.42	
hcp	68	0.916		−12		1.55 FM		11		2.71	1.91
hcp	80	0.921	−12		1.91 FM		−0.1		2.90		
hcp	85	0.924	−11		1.99 FM		4		2.92		

VIII. ELECTRONIC STRUCTURE IN THE IRON-CHROMIUM ALLOY SYSTEM

A. FeCr in the B2 crystal structure

For the remainder of the paper, we discuss the electronic structure of Fe-Cr alloys. It is very simple to construct a model for interactions between Fe and Cr by taking the geometric mean of the d-d hopping integrals and by moving the on-site d-orbital energies up and down by 0.1 Ry. Thereby, one would expect a small charge transfer from Cr to Fe, since the latter is more electronegative. To control this charge transfer, we apply a Hubbard U of 1 Ry. Our model deviates in this way slightly from the usual ansatz of local charge neutrality.[53]

The B2 alloy FeCr has a positive heat of formation and, hence, does not exist.[25,57] Nonetheless, it presents an interesting case in which to discuss the competition between ferro- and antiferromagnetism. One might expect this ordered alloy to be antiferromagnetic since the Cr sublattice could prefer to align antiferromagnetically with the neighboring Fe atoms. However, the nonmagnetic density of states clearly shows a large density of states at the Fermi level, and one expects the Stoner criterion to apply and lead to ferromagnetism. However, it turns out in the tight-binding model that both ferro- and antiferromagnetic solutions can be found depending on the value of the Hubbard U; but in the physically correct limit of large U, the alloy is ferromagnetic in agreement with the LSDA. To begin with, Fig. 9 shows Fe and Cr atom projected densities of states in nonmagnetic FeCr. We observe that the small amount of charge transfer permitted by the self-consistent tight binding leads to a closer agreement with the LDA than the non-self-consistent tight-binding density of states.

Figure 10 shows the density of states in the self-consistent spin-polarized tight-binding calculation employing a Hubbard U of 1 Ry. The result is in close agreement with the LSDA. The local moments on the Fe and Cr are $1.14\mu_B$ and $0.71\mu_B$, in reasonable accord with the estimated local moments in the LSDA, namely, $1.46\mu_B$ and $0.34\mu_B$. Figure 11 shows the local moments as a function of the Hubbard U where we find an unphysical regime if charge transfer is allowed to occur. In that case, we find an equal number of electrons in the spin up channel, while in the spin down, there is a larger population on the Fe site than the Cr site, leading to antiferromagnetism.

TABLE III. Energetics of Fe in the bcc and hcp crystal structures. Note that the tight-binding model incorrectly predicts that hcp is stable at $V/V_0=1$, but correctly reproduces the LSDA result that hcp is stable at $V/V_0=0.88$. The magnetic energies show that hcp is only very weakly antiferromagnetic, especially at high pressure, and this result is correctly reproduced by the tight-binding model.

	V/V_0	c/a	$\Delta E_{h\text{-}b}$ (mRy)		M (μ_B)			ΔE_{mag} (mRy)		K (Mbar)	
			TB	LSDA	TB	LSDA	Expt.	TB	LSDA	TB	Expt.
bcc	1	—	0	0	2.18 FM	2.08 FM	2.21 FM	17	30	2.24	1.68
hcp	1	1.63	−10	+6	1.8 AFM	1.57 AFM		3.2	1.1		
hcp	0.88	1.58	−7	−15	0.9 AFM	0.04 AFM		∼0	∼0		

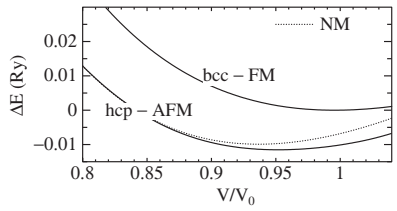

FIG. 8. Energy volume curves in Fe using the *spd* tight-binding model of Table I. We used hcp having ideal axial ratio. The dotted line shows nonmagnetic hcp; the two curves merge as the antiferromagnetic moment vanishes with reducing atomic volume.

B. Chromium as a dilute impurity in iron

While FeCr is ferromagnetic, a Cr atom in dilute concentration in Fe becomes antiferromagnetically ordered with respect to the Fe host atoms.[25] We find that the self-consistent tight-binding model reproduces the LSDA remarkably well in detail, and, furthermore, offers an explanation rather more readily than the LSDA. We illustrate this using a unit cell of 16 sites in the bcc-Fe lattice, in one site of which an Fe atom is replaced with a Cr atom. In Fig. 12, we show local densities of states projected onto the Cr and its neighboring Fe atoms, both using LSDA and tight binding. Note how the local density of states projected onto the Fe atoms neighboring the Cr impurity is hardly different from that of bulk Fe. It

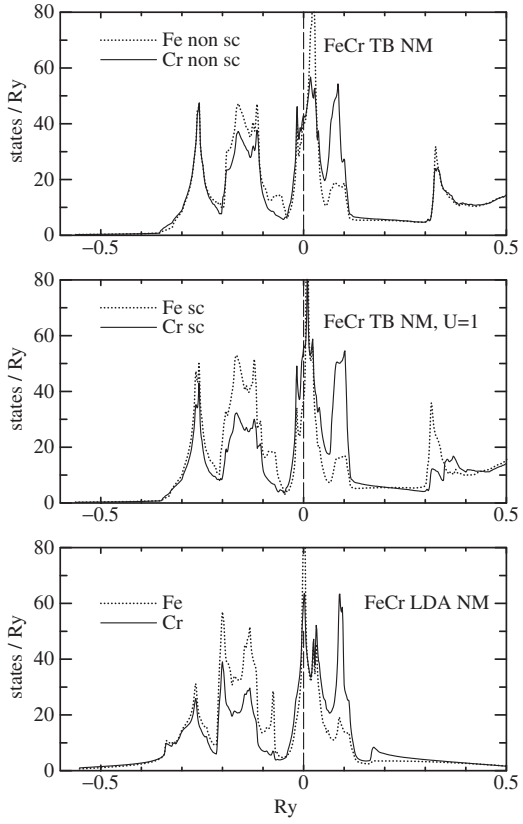

FIG. 9. Atom projected densities of states in nonmagnetic FeCr. The top panel shows a non-self-consistent tight-binding calculation in which the charge transfer is seen to be somewhat smaller than that found from the self-consistent tight-binding calculation in the center panel. This self-consistent result agrees better with the LDA in the lower panel.

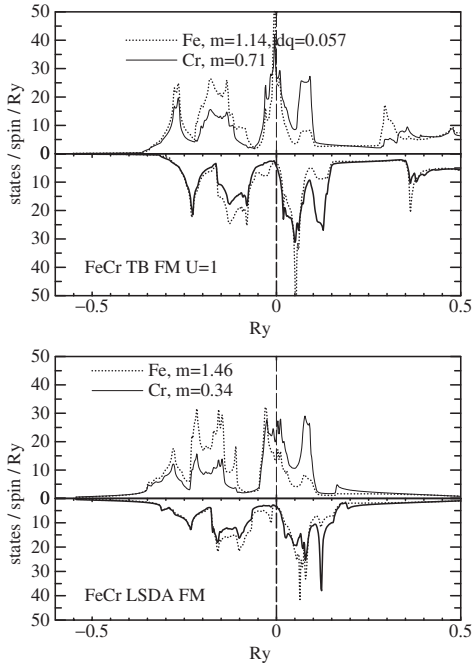

FIG. 10. Atom projected densities of states in ferromagnetic FeCr. The self-consistent tight-binding model is in close agreement with the LSDA.

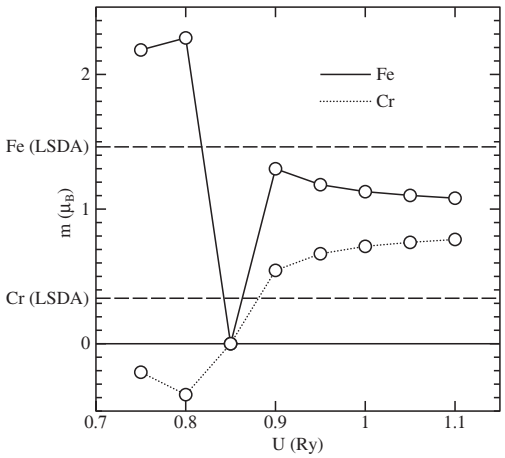

FIG. 11. Local magnetic moments (in μ_B) on the Fe and Cr atoms of B2 FeCr in the self-consistent tight-binding model as a function of the chosen Hubbard U parameter. For comparison, the estimated local moments from the LSDA are shown as horizontal lines (of course, the Hubbard U is "built into" the LSDA and cannot be varied. This may be regarded as an advantage and a disadvantage: in the tight binding, one may observe the role of parameters such as I and U by varying them). Note the transition from antiferro- to ferromagnetism as U is increased. The limit of local charge neutrality leads to rather smaller moments than found in the LSDA, but does predict the correct magnetic ordering.

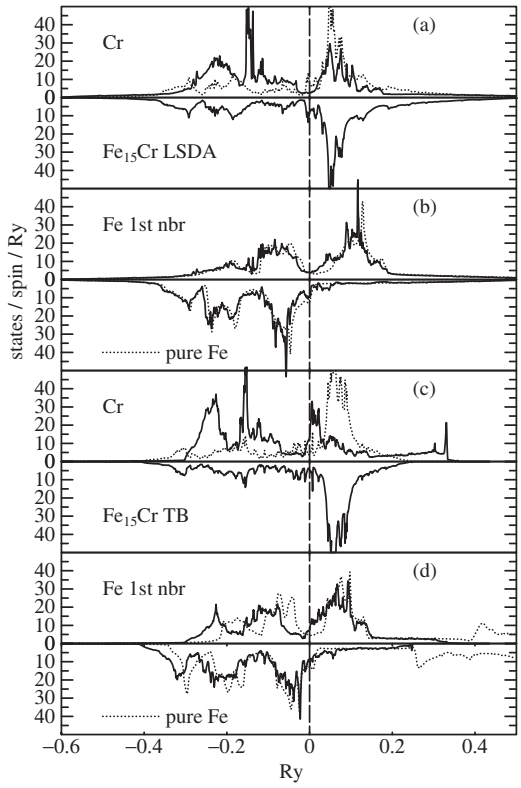

FIG. 12. Densities of states in an ordered $Fe_{15}Cr$ alloy on the bcc lattice. (a) and (c) show the local density of states projected onto the Cr atom, respectively, using LSDA and tight binding. The minority spin density of states in the lower panel is repeated, using a dotted line, for comparison by reflection about the abscissa. (b) and (d) show the local density of states projected onto the Fe atoms neighboring the Cr, again using LSDA and tight binding, respectively. A dotted line shows the density of states in bulk Fe.

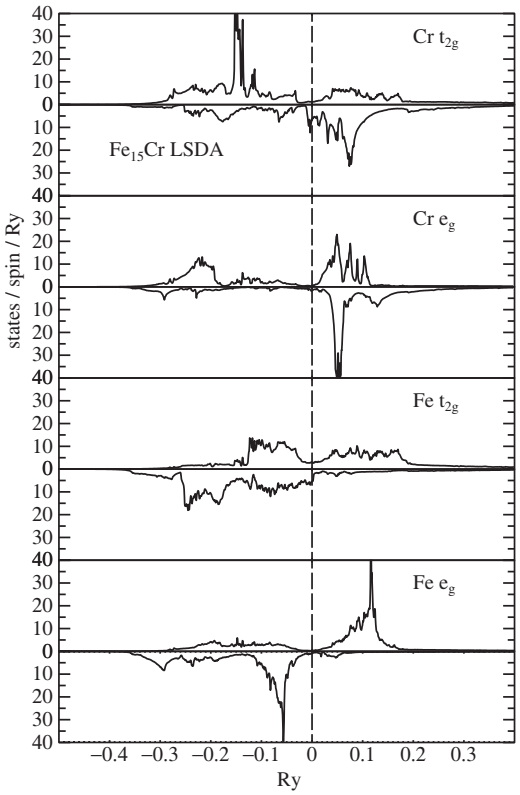

FIG. 13. LSDA local densities of states in $Fe_{15}Cr$ projected into the t_{2g} and e_g manifolds. This shows the nonbonding resonance on the Cr impurity to originate from the xy, yz, zx, and d orbitals.

is curious that the Fe does not accommodate itself to the presence of the Cr impurity. On the other hand, the Cr projected density of states is greatly perturbed from its bulk, as may be seen by comparison with Fig. 6. The most prominent feature is a virtual bound state in the occupied majority spins, which is almost completely unhybridized with the neighboring Fe minority spins. We show in Figs. 13 and 14 the densities of states from Fig. 12 projected into the t_{2g} and e_g manifolds. It becomes clear that this prominent feature arises from strongly localized states of xy, yz, and zx character.

IX. MAGNETIC FIXED MOMENT MODEL

It is clear from a comparison of Figs. 12 and 6 that a rigid band approximation would be a very poor description of alloying in the Fe-Cr system. A recent calculation using the coherent potential approximation in the LSDA has been made,[26] but in this case, the densities of states do not very well resemble those shown here in Fig. 12. However, we may use the magnetic fixed moment model described in Sec. III, in which the input density is constructed having a trial moment. Indeed, as seen in Fig. 14, such a trial density (to be described in detail below) gives a very faithful reproduction of the self-consistent density of states. In the simplest example, that of the nonmagnetic density of states of Fe shown in Fig. 3, a plot of ΔE_{mag} from Eq. (8) versus m is shown in Fig. 15, having the characteristic double-well[1] structure with minima at $m=2.3\mu_B$ and a magnetic energy of 21 mRy; these values may be compared with those from the *self-consistent* tight-binding calculation in Table III, viz. $2.18\mu_B$ and 17 mRy. The small discrepancies arise from the self-consistent calculation allowing the shape of the spin densities of states to be different from the input, non-self-consistent densities. As mentioned in the caption to Fig. 4 above, this is entirely due to the use of a nonorthogonal tight-binding model.

We can now use this simple construction to interpret the stability of the antiferromagnetic alignment of the Cr impurity in Fe. A trial spin-polarized density is constructed by imposing a moment of $+2.2\mu_B$ on each of the Fe atoms and a trial moment m on the Cr impurity. The associated band structure energy difference is found to which $\frac{1}{4}Im^2$ is added, in which we take $I=50$ mRy from Table I. The magnetic energy plotted against m is shown in Fig. 16.

Only one, antiferromagnetic, solution is found, having a local Cr moment of $2.42\mu_B$, which is close to the moment of $2.37\mu_B$ found in the self-consistent tight-binding calculation. (The estimated Cr local moment from our LSDA calculation is $2.08\mu_B$.) Although there is no ferromagnetic solution, it is instructive to plot the trial densities of states for trial local

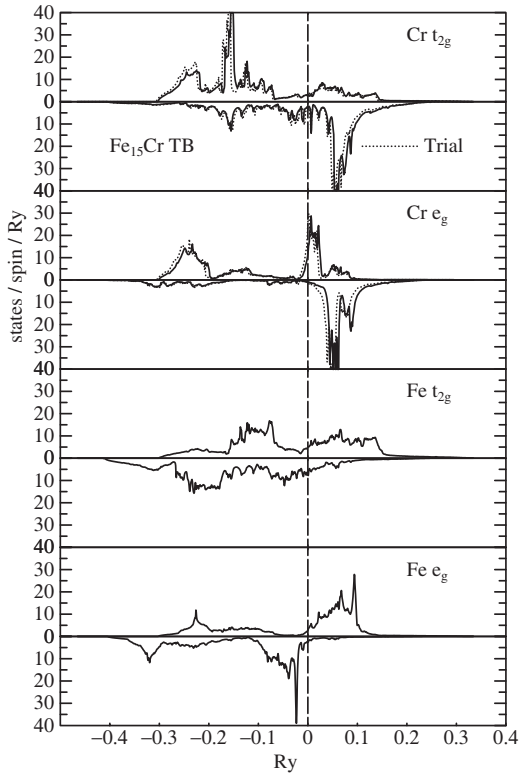

FIG. 14. As in Fig. 13, but using the tight-binding model. In the upper panel, a dotted line shows the density of states arising from a trial *input* non-self-consistent density with imposed moments on the Fe and Cr atoms (see the text). Note, first, the excellent detailed agreement with the LSDA in Fig. 13 and, second, the close similarity between the self-consistent and non-self-consistent densities of states.

moments of $2.37\mu_B$ in both antiferro- and ferromagnetic alignments. These are shown in Fig. 17. Neither looks at all like the density of states of pure Cr in Fig. 6; this is because to develop an antiferromagnetic state requires the cooperation of two sublattices, which cannot be achieved by isolated Cr atoms or small clusters of these (say, fewer than nine atoms) in a bcc-Fe host. This is why it is the Cr density of states that has to accommodate itself to the underlying Fe

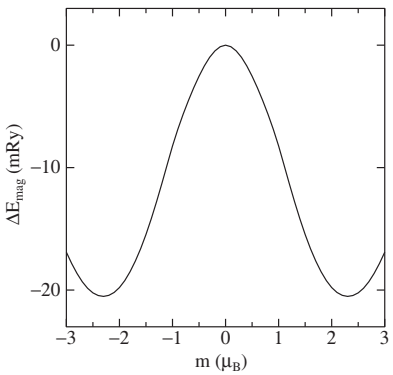

FIG. 15. Magnetic energy versus trial moment in the rigid band Stoner model for bcc-Fe (cf. Fig. 2). Curves of this type were first computed by Slater (Ref. 38).

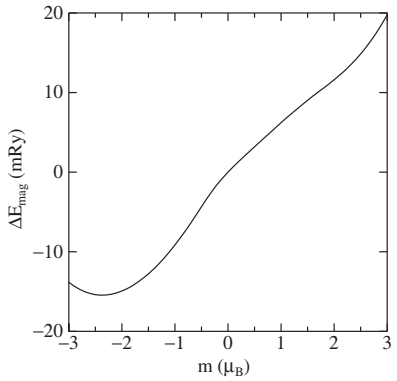

FIG. 16. Magnetic energy versus trial local Cr impurity moment in $Fe_{15}Cr$. Note there is only one antiferromagnetic solution.

electronic structure, and this lies at the heart of understanding the enthalpy of mixing and the phase diagram in the Fe-Cr system. Figure 17 helps explain why isolated Cr impurities do not align themselves ferromagnetically with the host Fe. To do so would require a density of states essentially that of pure *ferromagnetic* Cr, and this phase is unstable with respect to the observed antiferromagnetic phase in Cr. The alternative is to align antiferromagnetically, and this causes the density of states to adopt a shape quite unlike that in pure Cr, while, at the same time, there is a complete lack of cooperation from the very stable bcc-Fe density of states, practically the same as pure Fe even on the Fe atoms neighboring the impurity.

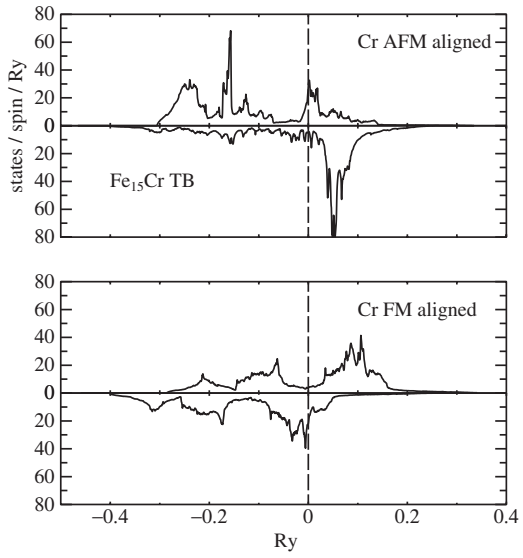

FIG. 17. Trial densities of states constructed by imposing fixed magnetic moments onto the Cr impurity in $Fe_{15}Cr$. As already seen in Fig. 14, the trial density for the antiferromagnetic alignment is very close to the corresponding self-consistent density of states. Because there is no energy minimum at ferromagnetic alignment (see Fig. 16), such a density cannot be achieved in a self-consistent procedure. This illustrates the usefulness of this construction.

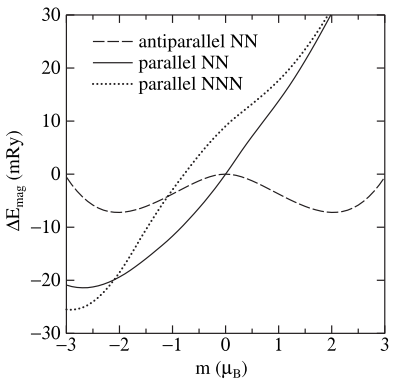

FIG. 18. Magnetic energy versus trial local Cr impurity moment in $Fe_{14}Cr_2$, having the two Cr atoms as nearest neighbors (NN) and next nearest neighbors along the cube diagonal (NNN). The solid line denotes the energy of the pair of Cr atoms having their spins aligned parallel to each other. The broken line refers to the two Cr having spins aligned antiparallel to each other. The dotted line is the energy in the case that the two Cr atoms are separated as next nearest neighbors. The zero of energy in this plot is the energy of the nonmagnetic NN case. Hence, the graph shows the lowering of energy as a result of moving the Cr atoms from NN to NNN positions *as long as spin polarization is permitted*. The repulsion between Cr impurities is thereby revealed, first, as a band structure effect and, second, as an effect of the magnetism.

X. ORIGIN OF THE REPULSION BETWEEN CHROMIUM IMPURITES AND THE ENTHALPY ANOMALY

Now we ask what is the stable magnetic structure of two Cr impurities placed as nearest neighbors in Fe? We go straight to the predictions of the tight-binding model shown in Fig. 18. We make trial spin densities having the Cr spins parallel or antiparallel to each other, and plot the magnetic energy as a function of their moment. In the case that they are antiparallel and assuming the two moments to have the same magnitude, we find a double well as expected. The more stable structure is for both spins to be aligned parallel to each other, but to be antiferromagnetically aligned with the spins of the Fe host. In fact, the antiparallel state is unstable, and we find that if the constraint is removed in a self-consistent calculation, this reverts to the parallel state.

If the Cr atoms are placed at next neighbor positions along the cube diagonal, with their spins aligned parallel to each other, we find an energy versus magnetic moment very similar to that of the single impurity in Fig. 16. In fact, our LSDA and tight-binding calculations (not presented here) show the densities of states and magnetic moments to be very similar in these two cases; indeed, the LSDA local Cr moment is a little larger in $Fe_{14}Cr_2$ than in $Fe_{15}Cr$ as seen also in the tight-binding model by comparing Figs. 16 and 18. This latter figure now illustrates rather clearly the origin of the repulsion between Cr impurities in bcc-Fe. The energy is *lower* when the atoms are placed at next nearest neighbor positions as long as spin polarization is allowed; otherwise, the energy ordering is reversed as is also found using LSDA calculations.[25] Furthermore, since the $\frac{1}{4}Im^2$ term is the same in both cases, this is clearly a *band structure effect*.

We can now offer a more detailed explanation for the anomaly in the enthalpy of mixing of Cr in Fe. In most of the concentration range, Cr prefers to cluster together to allow sufficient atoms to cooperate toward providing the two sublattices required to establish the antiferromagnetic state. Hence, the enthalpy of mixing is positive, and spinodal decomposition is observed.[22] Conversely, at low concentrations, the Cr may appear as isolated impurities stabilized by the change in spin-polarized density of states, which has quite a large weight at the bottom of the band as seen in Fig. 17. These isolated impurities *repel* each other, as already found by Klaver *et al.*,[25] shown clearly in our Fig. 18; hence, at low concentrations, the enthalpy of mixing is negative, but only while the concentration of Cr is sufficiently low for the Cr-Cr repulsion to dominate. Our present modeling explains the nearest neighbor repulsion in detail. The LSDA calculations[25] also showed that the Cr-Cr repulsion extends to second neighbors and beyond, these longer ranged interactions contribute significantly to the total repulsive energy of a pair; furthermore, they are present even when the system is forced to be non-spin-polarized, when the nearest neighbor repulsion collapses. An explanation of the longer ranged repulsion remains to be found in the band structure.

XI. CONCLUSIONS

We have described how itinerant magnetism can be incorporated into our self-consistent polarizable ion tight-binding model. This results in an additional parameter, the Stoner I, which we identify as minus twice the curvature of the exchange and correlation energy as a function of magnetic moment. A first order expansion of the Hohenberg-Kohn functional leads to a magnetic fixed moment model. We show that a very simple parametrization of the tight-binding model is possible, which will give a faithful reproduction of the energetics and electronic structure of the LSDA. The parameters of the model are easily transferable between the first row transition metals and their alloys. The simplest form of pair potential is quite adequate, except in the case of Fe, to reproduce structural stability and bulk modulus. Armed with this model, we address outstanding questions related to solution and clustering of Cr impurities in bcc-Fe. The fixed moment approach proves to be very useful in reproducing LSDA results and predicting magnetic structure and energy of complex transition metal alloy systems. This provides a powerful framework within which to explore complex magnetic structures in transition metals generally. The model is based on the correct physical picture, namely, itinerant magnetism resulting from a competition between kinetic, or band, energy described by intersite one-electron hopping matrix elements of the non-self-consistent tight-binding Hamiltonian and on-site exchange and correlation parametrized through a single Stoner parameter. Because the tight-binding approximation is particularly simple and transparent, we believe that this approach will find a number of applications in this area in the future.

ACKNOWLEDGMENTS

We are very grateful to David G. Pettifor for helpful comments on the paper. This work was supported by EPSRC under Grants No. GR/S80165/01 and No. GR/S81179/01.

APPENDIX A: CONNECTION TO LDA+U

We may arrive at an expression similar to Eq. (5) from the starting point of the theory of LDA+U.[58] The usual notation is to write n_m^σ for the number of electrons or occupation number in, say, a d band with quantum number m (not to be confused with the magnetic moment) and spin σ. Then defining U and J as spheridized, orbital independent Coulomb and exchange integrals, the on-site electron-electron interaction energy is[58–62]

$$E^U = \frac{1}{2}U\sum_{mm'\sigma} n_m^\sigma n_{m'}^{-\sigma} + \frac{1}{2}(U-J)\sum_{\substack{mm'\sigma \\ m\neq m'}} n_m^\sigma n_{m'}^\sigma$$

$$= \frac{1}{2}U\rho^2 - \frac{1}{2}J\sum_\sigma (\rho^\sigma)^2 - \frac{1}{2}(U-J)\sum_{m\sigma}(n_m^\sigma)^2. \quad \text{(A1)}$$

The first line shows in its first term unlike spins interacting through the Hubbard U, and in the second term, like-spin electrons interacting through a Hubbard term reduced by an amount J, as explained at the end of Sec. II. This term explicitly requires $m\neq m'$ in the sum: as two electrons cannot occupy the same state according to the Pauli principle, this would, otherwise, give an interaction between an electron and itself. Hence, the on-site electron-electron interaction properly includes the so-called self-interaction correction present in Hartree-Fock theory, but not in the LSDA.[63] The second line[61] follows directly after some algebra, expressing

$$\rho = \sum_{m\sigma} n_m^\sigma, \quad \rho^\sigma = \sum_m n_m^\sigma.$$

The three terms resulting in the second line of Eq. (A1) are, respectively, a direct Coulomb term, an exchange term, and a term which is of lower order of magnitude compared to the first two and which would amount to admitting an *orbital dependent* potential. In the spirit of the LSDA, we neglect[64] this last term and, by differentiation, we find for the potential seen by an electron with spin σ as a result of electron-electron interaction,

$$V^\sigma = \frac{\partial E^U}{\partial \rho^\sigma} = U\rho - J\rho^\sigma,$$

and so the exchange splitting between up and down spin energy levels is approximately $\Delta\varepsilon \sim V^+ - V^- = -J(\rho^+ - \rho^-) = -Jm$. After some further algebra, again neglecting the third term in Eq. (A1), we may also write

$$E^U = \frac{1}{2}\left(U - \frac{1}{2}J\right)\rho^2 - \frac{1}{4}Jm^2, \quad \text{(A2)}$$

which is equivalent to our expression (5) for E_2^U in Sec. II after identifying the exchange integral J with the Stoner parameter I. Note, however, that E^U is not an energy to second order in any charge density difference, but it could be cast into such a form if we make an expansion of the total energy in a generalized mean field multiband Hubbard model. We wish to emphasize two points here. (i) Both exchange *and* correlation are contained in Eqs. (5) and (A2) the effective Coulomb integral being reduced to $U-\frac{1}{2}J$ by exchange. Indeed, it is well known that the exchange-only Kohn-Sham-Gaspar potential gives a poor description of itinerant magnetism by overestimating the tendency to magnetism in transition metals.[16] (ii) As in LSDA, Eqs. (5) and (A2) are functionals of the spin density only and lead to orbital independent potentials. It is clear, though, from the foregoing how to recover the self-interaction correction (at least, in on-site terms in the Hamiltonian) in a tight-binding context, in which the potential seen by an electron is orbital dependent.

APPENDIX B: NONORTHOGONAL SELF-CONSISTENT TIGHT BINDING

There is a number of benefits of adopting a nonorthogonal tight-binding basis. It is widely believed to result in a more transferable model. In addition, it admits the concept of *bond charge*.[10] As we now demonstrate, this allows the self-consistency to adjust the hopping integrals as well as on-site matrix elements of the Hamiltonian. We recall that our self-consistent polarizable ion tight-binding model[18,19,66] is couched in terms of multipole moments of charge with respect to neutral, spherical atoms having $q_{\mathbf{R}}^0$ valence electrons. Hence, the self-consistent charge transfer to a site labeled by its position $\mathbf{R}$ in units of electron charge e is

$$\delta q_{\mathbf{R}} = q_{\mathbf{R}} - q_{\mathbf{R}}^0 \equiv Q_{\mathbf{R}0}. \quad \text{(B1)}$$

Higher moments of the charge develop as a result of crystal field splitting, and these are denoted $Q_{\mathbf{R}L}$, in which L is a composite index subsuming both angular momenta: $L=\{\ell m\}$. The Madelung potential (energy) at site $\mathbf{R}$ due to multipoles at sites $\mathbf{R}'$ is

$$V_{\mathbf{R}L}^M = e^2 \sum_{\mathbf{R}'\neq\mathbf{R}} \sum_{L'} B_{LL'}(\mathbf{R}'-\mathbf{R}) Q_{\mathbf{R}'L'}. \quad \text{(B2)}$$

$\mathbf{B}$ is a generalized Madelung matrix,[11,66] related to the structure constants of linear muffin-tin orbital (LMTO) theory.[14] For monopole interactions, we write

$$B_{00}(\mathbf{R}'-\mathbf{R}) = \frac{1}{|\mathbf{R}'-\mathbf{R}|} \equiv U_{\mathbf{R}\mathbf{R}'}.$$

The transfer of charge is resisted by a "Hubbard potential,"

$$V_{\mathbf{R}}^U = U_{\mathbf{R}} Q_{\mathbf{R}0}.$$

In the orthogonal self-consistent tight-binding model, these potentials are used to adjust the on-site matrix elements of the Hamiltonian, both on-site energies and off-diagonal crystal field terms. The increments to the Hamiltonian are

$$V_{\mathbf{R}L\mathbf{R}L'} = V_{\mathbf{R}}^U \delta_{LL'} + \sum_{L''} V_{\mathbf{R}L''}^M \Delta_{\ell\ell'\ell''} C_{LL'L''},$$

in which $C_{LL'L''}$ are the Gaunt coefficients that enforce the selection rules, and $\Delta_{\ell\ell'\ell''}$ are new parameters controlling the

strength of the crystal field splitting.[11,18,66] These may be adjusted, for example, to reproduce crystal field splittings in *ab initio* band structures or dipole moments in molecules.

If we include an overlap matrix $S_{\mathbf{R}L\mathbf{R}'L'}$, then solving the generalized eigenproblem leads to normalized eigenvectors $C^{n\mathbf{k}}_{\mathbf{R}L}$, and the charge at site $\mathbf{R}$ is

$$q_{\mathbf{R}} = \frac{1}{2}\sum_{n\mathbf{k}} f_{n\mathbf{k}} \sum_{\mathbf{R}'L'L} (\bar{C}^{n\mathbf{k}}_{\mathbf{R}L} S^{\mathbf{k}}_{\mathbf{R}L\mathbf{R}'L'} C^{n\mathbf{k}}_{\mathbf{R}L} + \text{c.c.})$$

$$= \sum_{n\mathbf{k}} f_{n\mathbf{k}} \sum_{L'L} |C^{n\mathbf{k}}_{\mathbf{R}L}|^2 + \frac{1}{2}\sum_{n\mathbf{k}} f_{n\mathbf{k}} \sum_{\mathbf{R}'L'L} (\bar{C}^{n\mathbf{k}}_{\mathbf{R}L} O^{\mathbf{k}}_{\mathbf{R}L\mathbf{R}'L'} C^{n\mathbf{k}}_{\mathbf{R}L} + \text{c.c.}).$$

Here, a bar and "c.c." imply complex conjugation. $f_{n\mathbf{k}}$ are occupation numbers[67] of the state at wave vector $\mathbf{k}$ and band index n, as used, say, in Fermi-Dirac or generalized Gaussian Brillouin zone integration,[68] or the linear tetrahedron method.[69] The final term amounts to a bond charge which is absent in orthogonal tight-binding models. To extract the bond charge explicitly, we have defined $\mathbf{O}=\mathbf{S}-\mathbf{1}$ and, since the norm is conserved separately at each $\mathbf{k}$ point, we work with Bloch transformed matrices, such that, for example,

$$S^{\mathbf{k}}_{\mathbf{R}L\mathbf{R}'L'} = \sum_{\mathbf{T}} S_{\mathbf{R}+\mathbf{T}L\mathbf{R}'L'} e^{i\mathbf{k}\cdot\mathbf{T}},$$

where $\mathbf{T}$ are the translation vectors of the crystal lattice.

For simplicity, we allow the overlap to make contributions only to the monopole moments of the charge; higher moments are defined as in the orthogonal case so that for $\ell > 0$, we have[11,18,19,66]

$$Q_{\mathbf{R}L} = \sum_{n\mathbf{k}} f_{n\mathbf{k}} \sum_{L'L''} \bar{C}^{n\mathbf{k}}_{\mathbf{R}L'} C^{n\mathbf{k}}_{\mathbf{R}L''} \Delta_{\ell\ell'\ell''} C_{LL'L''}.$$

We now find increments to the hopping integrals as a result of the self-consistent redistribution of bond charge. These are[11]

$$V^{\mathbf{k}}_{\mathbf{R}L\mathbf{R}'L'} = \frac{1}{2}(D_{\mathbf{R}} + D_{\mathbf{R}'}) O^{\mathbf{k}}_{\mathbf{R}L\mathbf{R}'L'},$$

where

$$D_{\mathbf{R}} = V^U_{\mathbf{R}} + \sum_{\mathbf{R}'} U_{\mathbf{R}\mathbf{R}'} Q_{\mathbf{R}'0}.$$

To preserve the norm, these need to be updated directly into the Bloch transformed Hamiltonian. Note that only monopole terms enter here as a result of our definition of the higher multipoles without reference to the overlap. $D_{\mathbf{R}}$ is the sum of Hubbard and point-charge Madelung potentials at site $\mathbf{R}$.

There are also additional terms in the interatomic forces. According to the Hellmann-Feynman theorem, the force is obtained from the derivative of the energy, taken while keeping the wave function frozen. In an orthogonal tight-binding model, multipole moments do not change under this constraint when the atom at $\mathbf{R}$ is displaced; hence, the only contribution to the force from self-consistent, second order terms in the energy is the classical electrostatic term,

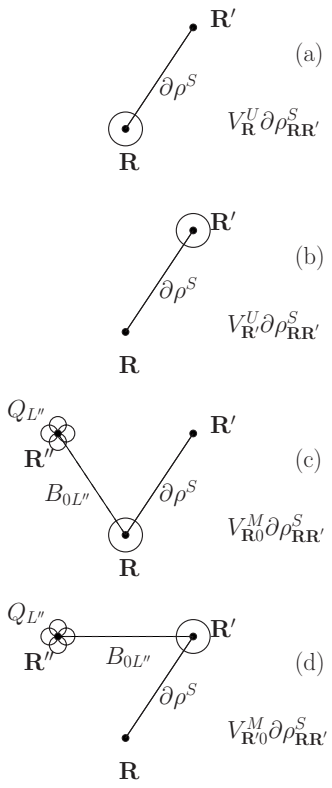

FIG. 19. Hubbard and Madelung contributions to the force on atom $\mathbf{R}$. Circles are intended to represent changes in monopoles arising from the displacement of the atom at $\mathbf{R}$, which modifies the charge on both sites $\mathbf{R}$ and $\mathbf{R}'$ through the scaling of the overlap matrix elements with bond length.

$$\mathbf{F}^{\text{es}}_{\mathbf{R}} = -\frac{1}{2}e^2 \sum_{\substack{\mathbf{R}'\neq\mathbf{R}'' \\ L'L''}} Q_{\mathbf{R}'L'} \frac{\partial B_{L'L''}(\mathbf{R}''-\mathbf{R}')}{\partial \mathbf{R}} Q_{\mathbf{R}''L''}.$$

However, in a *nonorthogonal* model, even at fixed eigenvectors, displacement of an atom will lead to changes in the bond charges with its neighboring atoms as a result of the changes in the overlap matrix elements. There are two additional contributions to the interatomic force. Since we are concerned with derivatives of the overlap matrix, we will require the quantity

$$\partial\rho^S_{\mathbf{R}\mathbf{R}'} = \sum_{LL'} \partial\rho^S_{\mathbf{R},\mathbf{R}L\mathbf{R}'L'},$$

where

$$\partial\rho^S_{\mathbf{R},\mathbf{R}L\mathbf{R}'L'} = -\partial\rho^S_{\mathbf{R}',\mathbf{R}L\mathbf{R}'L'}$$

$$= \frac{1}{2}\sum_{n\mathbf{k}} f_{n\mathbf{k}} \left(\bar{C}^{n\mathbf{k}}_{\mathbf{R}L} \frac{\partial S^{\mathbf{k}}_{\mathbf{R}L\mathbf{R}'L'}}{\partial \mathbf{R}} \bar{C}^{n\mathbf{k}}_{\mathbf{R}'L'} + \text{c.c.} \right).$$

Then, for the first contribution, we find

$$\mathbf{F}^U_{\mathbf{R}} = -\sum_{\mathbf{R}'} (V^U_{\mathbf{R}} + V^U_{\mathbf{R}'}) \partial\rho^S_{\mathbf{R}\mathbf{R}'},$$

and for the Madelung contribution,

$$\mathbf{F}_{\mathbf{R}}^{M} = -\sum_{\mathbf{R}'} (V_{\mathbf{R}0}^{M} + V_{\mathbf{R}'0}^{M}) \partial \rho_{\mathbf{R}\mathbf{R}'}^{S}.$$

$V_{\mathbf{R}}^{U}$ is the Hubbard potential, and $V_{\mathbf{R}0}^{M}$ is the $\ell=0$ component of the electrostatic potential (B2) seen at $\mathbf{R}$. These two contributions to the interatomic force are open to quite a simple interpretation if we make reference to Fig. 19.

When the atom at $\mathbf{R}$ moves, its own monopole moment changes by virtue of overlap with an atom at $\mathbf{R}'$. This leads to a change in Hubbard potential (energy) at site $\mathbf{R}$ and, hence, a force [Fig. 19(a)]. This change in monopole moment at $\mathbf{R}$ will result in a modified electrostatic interaction with a multipole moment at a third site $\mathbf{R}''$ (including the possibility $\mathbf{R}''=\mathbf{R}'$) described by the matrix element $B_{0L''}(\mathbf{R}''-\mathbf{R})$. This leads to the first Madelung contribution, shown in Fig. 19(c). The same movement also induces a change in the monopole moment at site $\mathbf{R}'$, giving rise to the second Hubbard contribution, shown in Fig. 19(b). The second Madelung contribution, illustrated in Fig. 19(d), corresponds to the force associated with the electrostatic interaction between a multipole at $\mathbf{R}''$ (admitting the possibility that $\mathbf{R}''=\mathbf{R}$) and the modified charge at $\mathbf{R}'$ through the Madelung matrix element $B_{0L''}(\mathbf{R}''-\mathbf{R}')$.

[1] S. L. Dudarev and P. M. Derlet, J. Phys.: Condens. Matter **17**, 7097 (2005).
[2] O. K. Andersen, J. Madsen, U. K. Poulsen, O. Jepsen, and J. Kollár, Physica B & C **86**, 249 (1977).
[3] G. Liu, D. Nguyen-Manh, B.-G. Liu, and D. G. Pettifor, Phys. Rev. B **71**, 174115 (2005).
[4] R. Drautz and D. G. Pettifor, Phys. Rev. B **74**, 174117 (2006).
[5] P. Olsson, J. Wallenius, C. Domain, K. Nordlund, and L. Malerba, Phys. Rev. B **72**, 214119 (2005).
[6] G. J. Ackland, J. Nucl. Mater. **351**, 20 (2006).
[7] E. C. Stoner, Proc. R. Soc. London, Ser. A **165**, 372 (1938).
[8] J. Friedel, *The Physics of Metals: I. Electrons* (Cambridge University Press, Cambridge, England, 1969), Chap. 8.
[9] W. A. Harrison, *Electronic Structure and the Properties of Solids* (Freeman, San Francisco, 1980).
[10] D. G. Pettifor, *Bonding and Structure of Molecules and Solids* (Oxford University Press, Oxford, 1995).
[11] M. W. Finnis, *Interatomic Forces in Condensed Matter* (Oxford University Press, Oxford, 2003).
[12] D. M. Roy and D. G. Pettifor, J. Phys. F: Met. Phys. **7**, L183 (1977).
[13] W. Zhong, G. Overney, and D. Tománek, Phys. Rev. B **47**, 95 (1993).
[14] O. K. Andersen, O. Jepsen, and D. Glötzel, *Proceedings of the International School of Physics, LXXXIX Corso, Varenna*, edited by F. Bassani, F. Fumi, and M. P. Tosi (North-Holland, Amsterdam, 1985), Chap. 3, p. 59.
[15] N. E. Christensen, O. Gunnarsson, O. Jepsen, and O. K. Andersen, J. Phys. Colloq. **49**, 17 (1988).
[16] O. Gunnarsson, J. Phys. F: Met. Phys. **6**, 587 (1976).
[17] D. Yeşilleten, M. Nastar, T. A. Arias, A. T. Paxton, and S. Yip, Phys. Rev. Lett. **81**, 2998 (1998).
[18] M. W. Finnis, A. T. Paxton, M. Methfessel, and M. van Schilfgaarde, Phys. Rev. Lett. **81**, 5149 (1998).
[19] S. Fabris, A. T. Paxton, and M. W. Finnis, Phys. Rev. B **61**, 6617 (2000).
[20] P. C. Hohenberg and W. Kohn, Phys. Rev. **136**, B864 (1964).
[21] I. Mirebeau, M. Hennion, and G. Parette, Phys. Rev. Lett. **53**, 687 (1984).
[22] J. M. Hyde, M. K. Miller, M. G. Hetherington, A. Cerezo, G. D. W. Smith, and C. M. Elliott, Phys. Met. Metallogr. **43**, 3415 (1995).
[23] G. J. Ackland, Phys. Rev. Lett. **97**, 015502 (2006).
[24] A. Caro, D. A. Crowson, and M. Caro, Phys. Rev. Lett. **95**, 075702 (2005).
[25] T. P. C. Klaver, R. Drautz, and M. W. Finnis, Phys. Rev. B **74**, 094435 (2006).
[26] P. Olsson, I. A. Abrikosov, and J. Wallenius, Phys. Rev. B **73**, 104416 (2006).
[27] W. Kohn and L. J. Sham, Phys. Rev. **140**, A1133 (1965).
[28] C. Köhler, G. Seifert, U. Gerstmann, M. Elstner, H. Overhof, and T. Frauenheim, Phys. Chem. Chem. Phys. **3**, 5109 (2001).
[29] J. Harris, Phys. Rev. B **31**, 1770 (1985).
[30] W. M. C. Foulkes and R. Haydock, Phys. Rev. B **39**, 12520 (1989).
[31] J. C. Slater, Phys. Rev. **49**, 537 (1936).
[32] M. Shimizu, Proc. Phys. Soc. London **84**, 397 (1964).
[33] This is the same I as defined by Janak (Ref. 34) averaged inside the atomic sphere as long as we admit a misprint in his Eq. (4): the "two" should become a "half."
[34] J. F. Janak, Phys. Rev. B **16**, 255 (1977).
[35] W. E. Pickett, J. Korean Phys. Soc. **29**, S70 (1996).
[36] E. C. Stoner, Philos. Mag. **40**, 1018 (1933).
[37] E. C. Stoner, Proc. R. Soc. London, Ser. A **1546**, 656 (1936).
[38] J. C. Slater, Phys. Rev. **49**, 931 (1936).
[39] J. Friedel, Trans. Metall. Soc. AIME **230**, 616 (1964).
[40] D. G. Pettifor, J. Magn. Magn. Mater. **15-18**, 847 (1980).
[41] All our LSDA calculations are made using the full-potential LMTO method, see M. Methfessel, M. van Schilfgaarde, and R. A. Casali, in *Electronic Structure and Physical Properties of Solids: The Uses of the LMTO Method*, edited by H. Dreysse, Lecture Notes in Physics Vol. 535 (Springer-Verlag, Berlin, 2000), pp. 114–147, We employ the LSDA parametrization of von Barth and Hedin (Ref. 42), modified (Ref. 43) by Moruzzi et al.
[42] U. von Barth and L. Hedin, J. Phys. C **5**, 1629 (1972).
[43] V. L. Moruzzi, J. F. Janak, and A. R. Williams, *Calculated Electronic Properties of Metals* (Pergamon, New York, 1978).
[44] U. K. Poulsen, J. Kollár, and O. K. Andersen, J. Phys. F: Met. Phys. **9**, L241 (1976).
[45] A. R. Mackintosh and O. K. Andersen, *Electrons at the Fermi Surface* (Cambridge University Press, Cambridge, England, 1980), Chap. 5.
[46] H. M. Polatoglou and M. Methfessel, Phys. Rev. B **41**, 5898 (1990).
[47] A. T. Paxton, M. Methfessel, and H. M. Polatoglou, Phys. Rev. B

41, 8127 (1990).
[48] D. Spanjaard and M. C. Desjonquères, Phys. Rev. B **30**, 4822 (1984).
[49] J. H. Rose, J. R. Smith, F. Guinea, and J. Ferrante, Phys. Rev. B **29**, 2963 (1984).
[50] A. T. Paxton, J. Phys. D **29**, 1689 (1996).
[51] H. Hasegawa and D. G. Pettifor, Phys. Rev. Lett. **50**, 130 (1983).
[52] The earliest estimation of I was made by Slater (Ref. 31) using experimental atomic spectra. He obtained $I=68$ mRy for Ni, in very close agreement with the modern band structure result (Ref. 2) of 69 mRy.
[53] D. G. Pettifor, Solid State Phys. **40**, 43 (1987).
[54] R. L. Clendenen and H. G. Drickamer, J. Phys. Chem. Solids **25**, 865 (1964).
[55] P. Bagno, O. Jepsen, and O. Gunnarsson, Phys. Rev. B **40**, 1997 (1989).
[56] L. Stixrude, R. E. Cohen, and D. J. Singh, Phys. Rev. B **50**, 6442 (1994).
[57] D. J. Singh, J. Appl. Phys. **76**, 6688 (1994).
[58] V. I. Anisimov, F. Aryasetiawan, and A. I. Lichtenstein, J. Phys.: Condens. Matter **9**, 767 (1997).
[59] V. I. Anisimov, I. V. Solovyev, M. A. Korotin, M. T. Czyżyk, and G. A. Sawatzky, Phys. Rev. B **48**, 16929 (1993).
[60] S. L. Dudarev, G. A. Botton, S. Y. Savrasov, C. J. Humphreys, and A. P. Sutton, Phys. Rev. B **57**, 1505 (1998).
[61] A. G. Petukhov, I. I. Mazin, L. Chioncel, and A. I. Lichtenstein, Phys. Rev. B **67**, 153106 (2003).
[62] Anisimov *et al.* (Ref. 59) gave a particularly clear derivation of this expression for E^U, but note a misprint in their Eq. (8): the E is not the same as the E in their Eq. (5), but is intended as a substitute for the *last term* in the latter equation taking into account exchange in addition to the direct Coulomb interaction.
[63] The more general form

$$E^U = \frac{1}{2}\sum_{mm'\sigma} U_{mm'} n_m^\sigma n_{m'}^{-\sigma} + \frac{1}{2}\sum_{mm'\sigma} (U_{mm'} - J_{mm'}) n_m^\sigma n_{m'}^\sigma$$

accounts for self-interaction implicitly since $U_{mm}=J_{mm}$. It is reasonable in tight binding as in the atomic spheres approximation to adopt the spherical averaged U and J, in which case $m'=m$ must be excluded explicitly in the sum over like spins.
[64] If we retain this term, or its more precise rotationally invariant form (Refs. 58 and 60) we may construct a "tight-binding+U" model (Ref. 65) which admits an orbital dependent potential and amounts to a self-interaction correction, at least in the *on-site* electron-electron interaction.
[65] S. Sanna, B. Hourahine, T. Gallauner, and T. Frauenheim, J. Phys. Chem. **111**, 5665 (2007).
[66] M. W. Finnis, A. T. Paxton, M. Methfessel, and M. van Schilfgaarde, in *Tight Binding Approach to Computational Materials Science*, edited by P. E. A. Turchi, A. Gonis, and L. Colombo, MRS Symposia Proceedings No. 491 (Materials Research Society, Pittsburgh, 1998), p. 265.
[67] It is to be understood that these occupation numbers are divided by the total number of **k** points in the Brillouin zone, or scaled by the number and degeneracy of **k** points in the irreducible zone.
[68] G. Kresse and J. Furthmüller, Comput. Mater. Sci. **6**, 15 (1996).
[69] O. Jepsen and O. K. Andersen, Solid State Commun. **9**, 1763 (1971).